J Inf Process Syst, Vol.16, No.4, pp.774~783, August 2020
https://doi.org/10.3745/JIPS.04.0179

ISSN 1976-913X (Print)
ISSN 2092-805X (Electronic)

JOURNAL OF INFORMATION PROCESSING SYSTEMS JIPS

Localization of Subsurface Targets Based on Symmetric Sub-array MIMO Radar

Qinghua Liu*, Yuanxin He*, and Chang Jiang*

Abstract

For the issue of subsurface target localization by reverse projection, a new approach of target localization with different distances based on symmetric sub-array multiple-input multiple-output (MIMO) radar is proposed in this paper. By utilizing the particularity of structure of the two symmetric sub-arrays, the received signals are jointly reconstructed to eliminate the distance information from the steering vectors. The distance-independent direction of arrival (DOA) estimates are acquired, and the localizations of subsurface targets with different distances are realized by reverse projection. According to the localization mechanism and application characteristics of the proposed algorithm, the grid zooming method based on spatial segmentation is used to optimize the locaiton efficiency. Simulation results demonstrate the effectiveness of the proposed localization method and optimization scheme.

Keywords

Direction of Arrival (DOA), Ground Penetrating Radar (GPR), MIMO, Reverse Projection, Symmetric Sub-array

1. Introduction

Localization of subsurface targets is of great importance both in military and civilian applications. As a non-destructive detection technology, ground penetrating radar (GPR) [1-4] is widely used in the localization of subsurface targets by virtue of its repeatability and sensitivity to the electromagnetic characteristics of the medium. The information of location and contour of the subsurface target from the echoes are obtained through the analysis of transmitting and receiving electromagnetic waves. For a long time, single-input single-output (SISO) radar system was used to detect targets in most of the traditional GPR systems, which uses one antenna to emit electromagnetic signals and uses one antenna to receive echoes. Although SISO radar has the advantages of simple structure and easy hardware implementation, its detection performance is difficult to get greater improvement because of the limited amount of information. With the development of radar technology and the steady increase of application requirements, the multiple-input multiple-output (MIMO) radar has received extensive attentions [5-8]. It employs multiple antennas to emit orthogonal waveforms or non-coherent waveforms, and multiple antennas to receive the echoes reflected by the targets. Compared with the SISO radar system, by making full use of the spatio-temporal information of the targets, the detection performance can be improved qualitatively with the higher imaging resolution and stronger anti-interference ability. Conventional

Manuscript received January 9, 2020; first revision May 19, 2020; accepted May 24, 2020.

Corresponding Author: Qinghua Liu (liuqinghual@126.com)

* Guangxi Key Lab of Wireless Wideband Communication & Signal Processing, Guilin University of Electronic Technology, Guilin, China (liuqinghual@126.com, 598955611@qq.com, 912568584@qq.com)

localization methods of GPR are mostly based on range migration (RM) algorithm [9], reverse time migration (RTM) algorithm [10] and back projection (BP) algorithm [11]. Although the above algorithms can perform high-precision reconstruction of the detection area, the amount of data collected is large and the time for positioning is long. In order to locate the target more quickly, the algorithm based on parameter estimation such as MUSIC algorithm was used to achieve the localization of subsurface target, but it is based on conventional radar array. In [12], the parameter estimation of MIMO radar was applied to the localization of subsurface target, and the localization method of reverse projection based on 1D direction of arrival (DOA) estimation was proposed. Aiming at the simple target of subsurface, the data of multiple measuring points were used for rapid localization. However, this research is based on conventional linear array of MIMO radar, which contains coupling of 2D information between angle and distance in the steering vector of received signal. It cannot directly perform the 1D DOA estimation without distance dependence. When there are multi-targets with different distances, the localization results of reverse projection will be inaccurate. In order to solve the problem of angle-distance coupling in the steering vector of near-field, the stepwise procedure to estimate the distance and angle is realized by constructing the fourth-order cumulant, which needs to accumulate a large number of snapshots, and requires a great amount of computation, so it is not suitable for reverse projection.

A new approach of target localization of reverse projection with different distances based on symmetric sub-array MIMO radar is proposed in this paper. The distance information in the steering vector is eliminated by utilizing the particularity of structure of the symmetric sub-array. The rest of this paper is organized as follows. In Section 2, the signal model of symmetric sub-array MIMO radar is formulated with near-subsurface targets. In Section 3, the received signals of two sub-arrays are reconstructed jointly. In Section 4, the DOA estimation of the reconstructed signals is preformed, by which, the spectral amplitudes are provided for reverse projection. In Section 5, the proposed method is verified through the simulation and optimization experiments. Finally, conclusions are drawn in Section 6.

2. Signal Model

In order to simplify the analysis, it is assumed that the subsurface medium is a homogeneous and lossless single ideal medium. For lossy medium model, the following model is still applicable by adding attenuation factor [12]. Based on the above assumptions, a MIMO radar system which consists of two symmetric sub-arrays is considered. Each sub-array is a uniform linear array with N elements for both transmission and reception, as shown in Fig. 1. The coordinate origin O is set as the reference point. The two sub-arrays are symmetrically distributed with the reference point. The distance between the first array element of each sub-array to the reference point is D, and the distance between the adjacent antenna elements of each sub-array is d. It is assumed that there exists a target p in the underground space and its reflection coefficient is β_p. The distance between the target and the coordinate origin is r_p, and the angle between the target and the normal direction of the array at the origin is θ_p. The distance from the n-th element to the target in sub-array X and Y are $r_{x,n}$ and $r_{y,n}$, respectively. The distance from the target to the m-th element are $r_{x,m}$ and $r_{y,m}$, respectively, where $n = 1, 2, \cdots, N$ and $m = 1, 2, \cdots, N$.

Each array element of the MIMO radar transmits mutually orthogonal narrowband signals. The transmitted signals of the n-th element of sub-array X and Y propagate in the subsurface medium and are received by the their respective m-th element after reflected by the target p. The received signals $x_{n,m}(t)$ of sub-array X and $y_{n,m}(t)$ of sub-array Y can be expressed as

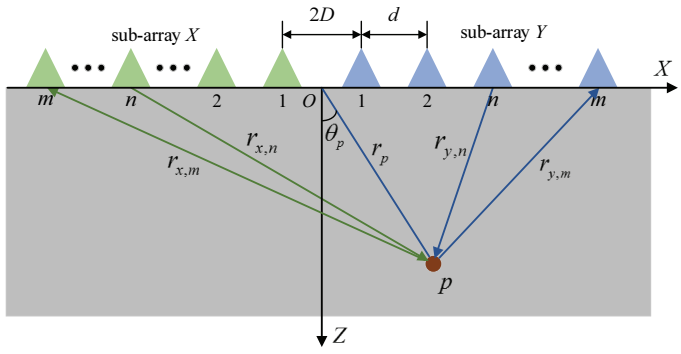

Fig. 1. Model of GPR based on two symmetric sub-arrays.

$$\begin{aligned} x_{n,m}(t) &= a_{r,x,m}(\theta_p, r_p)\beta_p a_{t,x,n}(\theta_p, r_p)s_{x,n}(t) + n_{x,n,m}(t) \\ y_{n,m}(t) &= a_{r,y,m}(\theta_p, r_p)\beta_p a_{t,y,n}(\theta_p, r_p)s_{y,n}(t) + n_{y,n,m}(t) \end{aligned} \tag{1}$$

where $s_{x,n}(t)$ and $s_{y,n}(t)$ represent the transmitted source signals of the n-th element of sub-array X and Y, $n_{x,n,m}(t)$ and $n_{y,n,m}(t)$ denote the noise parts contained in the received signals, respectively. The steering factors are written as

$$a_{r,x,m}(\theta_p, r_p) = \exp\left(j2\pi f_0\left(r_{x,m} - r_p\right)/v\right) \qquad a_{t,x,n}(\theta_p, r_p) = \exp\left(j2\pi f_0\left(r_{x,n} - r_p\right)/v\right) \tag{2}$$

$$a_{r,y,m}(\theta_p, r_p) = \exp\left(j2\pi f_0\left(r_{y,m} - r_p\right)/v\right) \qquad a_{t,y,n}(\theta_p, r_p) = \exp\left(j2\pi f_0\left(r_{y,n} - r_p\right)/v\right) \tag{3}$$

where f_0 is the radiation frequency of the radar, v denotes the propagation speed of electromagnetic waves in the underground medium, which is related to the relative dielectric constant of the medium. The specific expression of v is described as

$$v = c/\sqrt{\varepsilon_r} \tag{4}$$

where c is the propagation speed of electromagnetic waves in vacuum, ε_r is the relative dielectric constant of the underground medium. In the above model, according to the geometric relation between the target and each element of two sub-arrays, it can be concluded as

$$\begin{aligned} r_{x,m} &= \sqrt{r_p^2 + \left(D + (m-1)d\right)^2 + 2\left(D + (m-1)d\right)r_p \sin\theta_p} \\ r_{x,n} &= \sqrt{r_p^2 + \left(D + (n-1)d\right)^2 + 2\left(D + (n-1)d\right)r_p \sin\theta_p} \end{aligned}, \tag{5}$$

$$\begin{aligned} r_{y,m} &= \sqrt{r_p^2 + \left(D + (m-1)d\right)^2 - 2\left(D + (m-1)d\right)r_p \sin\theta_p} \\ r_{y,n} &= \sqrt{r_p^2 + \left(D + (n-1)d\right)^2 - 2\left(D + (n-1)d\right)r_p \sin\theta_p} \end{aligned}. \tag{6}$$

Thus, the receive and transmit steering vectors of the sub-array X are written as

$$\boldsymbol{a}_{r,x}(\theta_p, r_p) = \left[a_{r,x,1}(\theta_p, r_p), a_{r,x,2}(\theta_p, r_p), \cdots, a_{r,x,N}(\theta_p, r_p)\right]^{\mathrm{T}}, \tag{7}$$

$$\boldsymbol{a}_{t,x}(\theta_p, r_p) = \left[a_{t,x,1}(\theta_p, r_p), a_{t,x,2}(\theta_p, r_p), \cdots, a_{t,x,N}(\theta_p, r_p)\right]^{\mathrm{T}}. \tag{8}$$

Similarly, the receive and transmit steering vectors of the sub-array Y are described as

$$\boldsymbol{a}_{r,y}\left(\theta_p,r_p\right)=\left[a_{r,y,1}\left(\theta_p,r_p\right),a_{r,y,2}\left(\theta_p,r_p\right),\cdots,a_{r,y,N}\left(\theta_p,r_p\right)\right]^{\mathrm{T}}, \tag{9}$$

$$\boldsymbol{a}_{t,y}\left(\theta_p,r_p\right)=\left[a_{t,y,1}\left(\theta_p,r_p\right),a_{t,y,2}\left(\theta_p,r_p\right),\cdots,a_{t,y,N}\left(\theta_p,r_p\right)\right]^{\mathrm{T}}. \tag{10}$$

According to the above steering vectors, the vectors of the received signals of two sub-arrays can be expressed as follows:

$$\begin{aligned}\boldsymbol{x}&=\boldsymbol{a}_{r,x}\left(\theta_p,r_p\right)\beta_p\boldsymbol{a}_{t,x}^{\mathrm{T}}\left(\theta_p,r_p\right)\boldsymbol{s}_x+\boldsymbol{n}_x\\ \boldsymbol{y}&=\boldsymbol{a}_{r,y}\left(\theta_p,r_p\right)\beta_p\boldsymbol{a}_{t,y}^{\mathrm{T}}\left(\theta_p,r_p\right)\boldsymbol{s}_y+\boldsymbol{n}_y\end{aligned} \tag{11}$$

where $\boldsymbol{s}_x=\left[s_{x,1}(t),s_{x,2}(t),\cdots,s_{x,N}(t)\right]^{\mathrm{T}}$ and $\boldsymbol{s}_y=\left[s_{y,1}(t),s_{y,2}(t),\cdots,s_{y,N}(t)\right]^{\mathrm{T}}$ represent the transmitted signal vectors in Hadamard code, $\boldsymbol{n}_x\in C^{N\times N}$ and $\boldsymbol{n}_y\in C^{N\times N}$ denote the vectors of noise parts, respectively.

Since each transmitting element emits an orthogonal signal, it can be obtained the following equations:

$$\begin{aligned}\boldsymbol{s}_x\boldsymbol{s}_x^{\mathrm{H}}/L_s&=\boldsymbol{I}\\ \boldsymbol{s}_y\boldsymbol{s}_y^{\mathrm{H}}/L_s&=\boldsymbol{I}\end{aligned} \tag{12}$$

where L_S represents the number of snapshots, $\boldsymbol{I}$ denotes the unit matrix, and the superscript $(\cdot)^{\mathrm{H}}$ represents conjugate transpose operation. After the echo signal arrives at the receiving element, it is demodulated to the baseband, and separated by matched filter. At this time, the received signal of each sub-array can be expressed as

$$\begin{aligned}\boldsymbol{x}&=\boldsymbol{a}_{r,x}\left(\theta_p,r_p\right)\beta_p\boldsymbol{a}_{t,x}^{\mathrm{T}}\left(\theta_p,r_p\right)+\boldsymbol{n}_x\\ \boldsymbol{y}&=\boldsymbol{a}_{r,y}\left(\theta_p,r_p\right)\beta_p\boldsymbol{a}_{t,y}^{\mathrm{T}}\left(\theta_p,r_p\right)+\boldsymbol{n}_y\end{aligned}. \tag{13}$$

3. Signal Reconstruction

Performing a second-order Taylor expansion on Eqs. (5) and (6) to obtain their approximate values as below

$$\begin{aligned}r_{x,m}&=r_p+\left(D+(m-1)d\right)\sin\theta_p+\left(D+(m-1)d\right)^2\cos^2\theta_p/\left(2r_p\right),\\ r_{x,n}&=r_p+\left(D+(n-1)d\right)\sin\theta_p+\left(D+(n-1)d\right)^2\cos^2\theta_p/\left(2r_p\right)\end{aligned} \tag{14}$$

$$\begin{aligned}r_{y,m}&=r_p-\left(D+(m-1)d\right)\sin\theta_p+\left(D+(m-1)d\right)^2\cos^2\theta_p/\left(2r_p\right),\\ r_{y,n}&=r_p-\left(D+(n-1)d\right)\sin\theta_p+\left(D+(n-1)d\right)^2\cos^2\theta_p/\left(2r_p\right)\end{aligned}. \tag{15}$$

Substituting Eqs. (14) and (15) into the transmitting and receiving steering vectors, it can be obtained the following expression:

$$\left(\boldsymbol{a}_{r,x}\left(\theta_p,r_p\right)\boldsymbol{a}_{t,x}^{\mathrm{T}}\left(\theta_p,r_p\right)\right)\odot\left(\boldsymbol{a}_r\left(\theta_p\right)\boldsymbol{a}_t^{\mathrm{T}}\left(\theta_p\right)\right)=\boldsymbol{a}_{r,y}\left(\theta_p,r_p\right)\boldsymbol{a}_{t,y}^{\mathrm{T}}\left(\theta_p,r_p\right) \tag{16}$$

where $\odot$ represents the Hadamard product operation, and the steering vectors are described as

$$\begin{aligned}\boldsymbol{a}_r\left(\theta_p\right)&=\left[\exp\left(-j4\pi f_0D\sin\theta_p/v\right),\exp\left(-j4\pi f_0\left(D+d\right)\sin\theta_p/v\right),\cdots,\exp\left(-j4\pi f_0\left(D+(N-1)d\right)\sin\theta_p/v\right)\right]^{\mathrm{T}}\\ \boldsymbol{a}_t\left(\theta_p\right)&=\left[\exp\left(-j4\pi f_0D\sin\theta_p/v\right),\exp\left(-j4\pi f_0\left(D+d\right)\sin\theta_p/v\right),\ \cdots,\exp\left(-j4\pi f_0\left(D+(N-1)d\right)\sin\theta_p/v\right)\right]^{\mathrm{T}}\end{aligned}. \tag{17}$$

Obviously, Eq. (17) can be regarded as a far-field steering vectors of a uniform linear array MIMO radar with N elements and $2d$ element spacing. The transmit and receive steering vectors of the two sub-arrays are interrelated by Eq. (16), and Eq. (17) can be obtained by joint processing of received signals from the two sub-arrays.

The reconstructed signal $\boldsymbol{G}$ is calculated based on the Hadamard product of $\boldsymbol{x}^*$ and $\boldsymbol{y}$, where the superscript $(\cdot)^*$ denotes the conjugate operation. The reconstructed signals $\boldsymbol{G}$ can be expressed as

$$\boldsymbol{G}=\boldsymbol{a}_r\left(\theta_p\right)\beta_p^2\boldsymbol{a}_t^{\mathrm{T}}\left(\theta_p\right)+\boldsymbol{n}_G \tag{18}$$

where β_p^2 represents reflection coefficient of target after signal reconstruction, $\boldsymbol{n}_G$ represents noise contained in reconstructed signals. According to the above analysis, the reconstructed signals model is a far-field model of a uniform linear array MIMO radar with N elements and $2d$ element spacing. The receive and transmit steering vectors only contain angle information without distance information, and the DOA estimation can be directly performed for multi-targets with different distances from the reconstructed signals model.

4. Target Localization

In this section, the locations of targets are acquired by reverse project method from the amplitudes of DOA estimates. The classical Capon and MUSIC algorithms are used to estimate DOA of target. Other algorithms with higher accuracy can also be used to estimate DOA.

The principle of target localization by reverse projection is shown in Fig. 2. The normalized spectrum amplitudes of DOA estimates are obtained by the MIMO radar consisting of two symmetric sub-arrays at the measuring point 1. The normalized spectrum amplitudes are projected as pixel values to each position of the detection area, and the detection image is formed at the measuring point. It is obvious that image of single measuring point cannot determine the location of target. Therefore, the MIMO radar needs to be moved to the multiple measuring points to obtain the location of target by overlapping the multiple detection images.

After the detection image $I_k(X,Z)$ of the k-th measuring point is obtained, it is accumulated with all the detection images to obtain the final localization image $I_{all}(X,Z)$ as below,

$$I_{all}(X,Z)=\sum_{k=1}^{K}I_k(X,Z)\,. \tag{19}$$

where K is the number of the measuring points.

From the above analysis, the positioning accuracy is related with DOA estimates and the distribution of measuring points. The more accurate DOA estimate is, or the sharper spectrum peak is, the more accurate position estimation is. In a detection area, the measuring points should be evenly distributed to avoid local scan, while the distance between adjacent measuring points is slightly bigger than the length of array.

In the case of near subsurface, each array movement is accompanied by the change of the target DOA, which enables that the target location is achieved by using the reverse projection values of multiple positions. However, in the case of far-field, if the distance between the adjacent measuring points is relatively small, the DOA estimates obtained at different measuring points are almost the same, and target

positions cannot be located through the intersection points. Therefore, this reverse projection method is relatively suitable for near-field conditions.

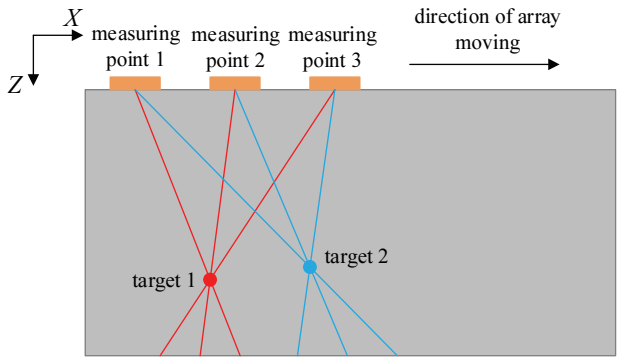

Fig. 2. Principle diagram of target localization by reverse projection.

5. Simulation

In this section, experiments are implemented to validate the effectiveness of the proposed approach. The simulations are performed according to the model of GPR based on symmetric sub-arrays shown in Fig. 1.

5.1 The Simulation of Localization of Multi-Targets

The element number of each sub-array is N=6. The relative dielectric constant of the underground medium is ε_r =9. The frequency of transmitted signal is f_0 =100 MHz. Considering the Fresnel approximation, the element spacing is d=0.25 m. The distance between the two sub-arrays is $2D$=d, so that the two sub-arrays form a uniform linear array of 12 elements. The data from 6 measuring points are collected, and the distance between adjacent measuring points is 0.6 m, with SNR=–10 dB and SNR=0 dB.

The situation of multi-targets with different distances is considered. In the following experiments, three point targets are selected that the coordinates are (0.75 m, 1.75 m), (1.50 m, 2.00 m), and (2.25 m, 1.50 m), respectively. The reflection coefficients of all targets are set to 1. Figs. 3(a), 3(b), 4(a) and 4(b) are the results of reverse projection before and after adding threshold of Capon algorithm with SNR=–10 dB and SNR=0 dB with the grid Δd=0.01 m, respectively. Figs. 3(c), 3(d), 4(c) and 4(d) are results of MUSIC algorithm with the same grid, respectively. The simulation results show that the symmetric sub-array MIMO radar realizes the localization of multi-targets with different distances by reverse projection, which verifies the effectiveness of the proposed method. The radial lines are eliminated by adding a threshold. From the results in Figs. 3 and 4, the performance of MUSIC algorithm is better than Capon algorithm, based on the fact that the sharper peaks of the former are sharper than that of the latter. In order to evaluate the imaging results more intuitively, the entropy value (ENT) is introduced to evaluate the complexity of the whole image. ENT is defined as the average number of bits of the gray level set of the image. The smaller the value, the clearer the image is. The result from Table 1 shows that the image is clearer and the positioning accuracy is higher after adding threshold by comparison of ENT. With the increase of SNR, the better the location result is.

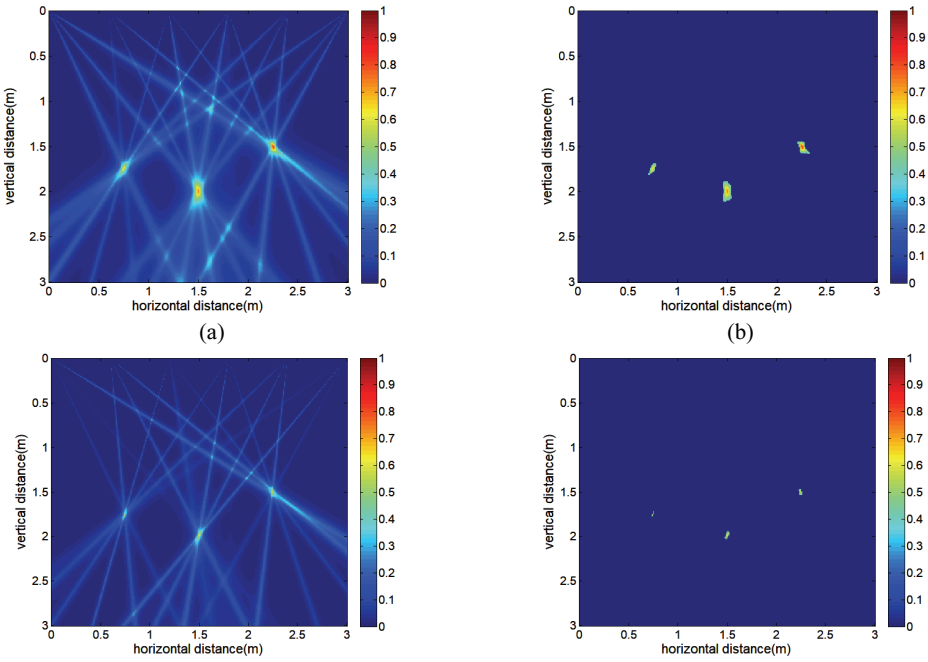

Fig. 3. Localization of multi-targets with SNR= –10 dB: (a) original image of reverse projection of Capon algorithm, (b) image of adding threshold of Capon algorithm, (c) original image of reverse projection of MUSIC algorithm, and (d) image of adding threshold of MUSIC algorithm.

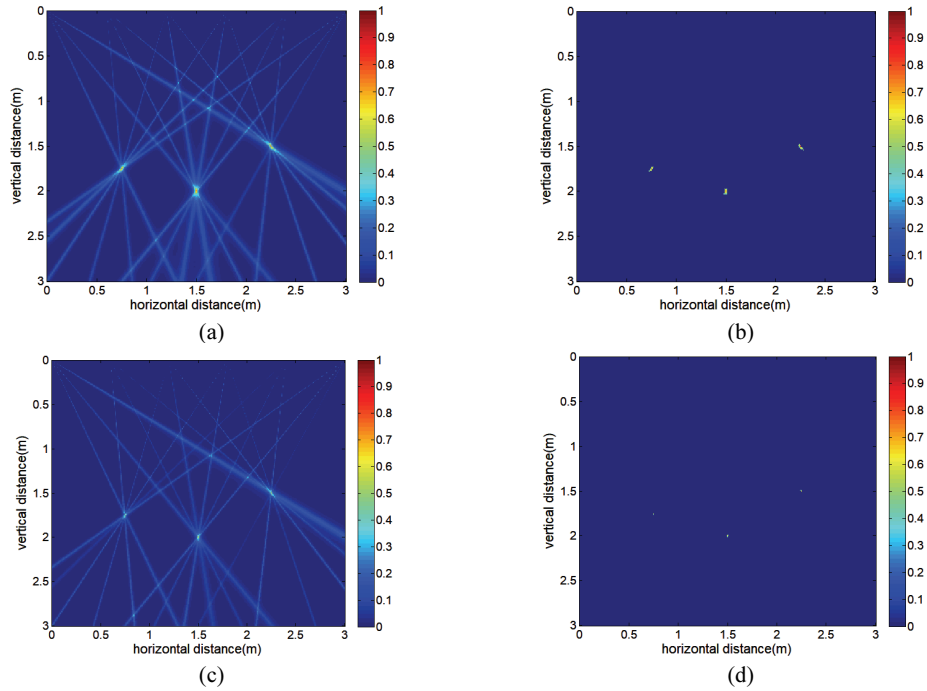

Fig. 4. Localization of multi-targets with SNR=0 dB, (a) original image of reverse projection of Capon algorithm, (b) image of adding threshold of Capon algorithm, (c) original image of reverse projection of MUSIC algorithm, (d) image of adding threshold of MUSIC algorithm.

Table 1. Comparison of ENT from Figs. 3 and 4

Algorithm	SNR (dB)	Before adding threshold	After adding threshold
Capon, Fig. 3(a) and 3(b)	-10	5.5632	0.0590
MUSIC, Fig. 3(c) and 3(d)	-10	4.9633	0.0101
Capon, Fig. 4(a) and 4(b)	0	3.9535	0.0096
MUSIC, Fig. 4(c) and 4(d)	0	2.6576	0.0016

5.2 The Simulation of Algorithm Optimization

Although the simulation results in the previous section have achieved the localization of multi-targets with different distances, it can be found that this method still has room for improvement in localization efficiency.

Different imaging resolutions should be adopted for different areas. Obviously, the target areas that we are interested in only occupy a small part of the entire detection area, therefor, the imaging resolution of the target areas are needed to increase. For non-target area, the redundant information is wanted to be discarded, and the imaging resolution is reduced.

By observing the relationship between the average program running time (APRT) and the grid spacing in Fig. 5, it can be seen that APRT decreases rapidly with the increase of grid spacing, which means that the imaging resolution has a great impact on the running time of the program. It shows that the optimization of algorithm efficiency can be effectively achieved by reducing the imaging resolution of non-target area on the premise of ensuring the high resolution of target area.

Based on the above analysis, simulation experiments are carried out on the detection area as below. The simulation parameters are consistent with the above simulation with SNR=–10 dB. The grid spacing in the low-resolution estimation of the entire detection area is Δd=0.05 m, and the grid spacing in the high-resolution estimation of the target area is Δd=0.01 m. The simulation results in Fig. 6 show that the target location is not accurately estimated under the low resolution, and the detail of the target area are missing, while the imaging result of the optimization algorithm still maintains a high resolution with the smaller value of APRT and the almost same value of ENT in Table 2.

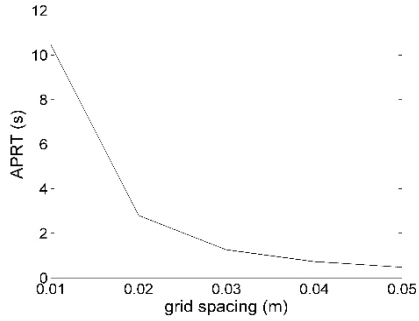

Fig. 5. Relationship between APRT and grid spacing (under the Inter i7-6700 processor using MATLAB R2013a).

Table 2. Comparison of simulation results

Capon algorithm	High-resolution imaging of entire area	High-resolution imaging of target area
APRT (s)	5.17	3.09
ENT (bit/pixel)	0.0953	0.0957

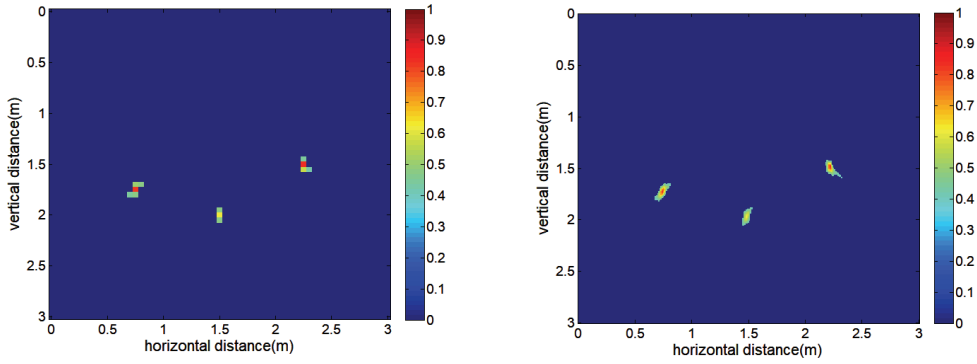

(a) (b)

Fig. 6. Localization of multi-targets of Capon algorithm with SNR= –10 dB: (a) low-resolution imaging the entire area of Δd=0.05 m and (b) high-resolution of the target area of Δd=0.01 m.

6. Conclusions

For the conventional linear array MIMO radar, the reverse projection method is unable to correctly locate multi-targets with different distances because of the coupling of distance and angle in near-field. The structure of symmetric sub-array is designed, and the received signals of two sub-arrays are jointly reconstructed in this paper. The reconstructed signals can realize the distance-independent DOA estimation, and the subsurface target localizations are obtained with different distances. On this basis, the grid zooming design of spatial segmentation is used to optimize the localization efficiency. The effectiveness of the proposed localization method and optimization schemes is verified by simulation results.

Acknowledgement

This paper is supported by the National Natural Science Foundation of China (No. 61861011), the Guangxi Natural Science Foundation (No. 2016GXNSFAA380036 and 2018GXNSFAA138091), and the Science and Technology on Near-Surface Detection Laboratory Foundation (No. TCGZ2017A010), and the Major Science and Technology Foundation of Guangxi Province (No. AA17204093).

References

[1] G. Kilic and L. Eren, "Neural network based inspection of voids and karst conduits in hydro–electric power station tunnels using GPR," *Journal of Applied Geophysics*, vol. 151, pp. 194-204, 2018.

[2] F. H. C. Tivive, A. Bouzerdoum, and C. Abeynayake, "GPR target detection by joint sparse and low-rank matrix decomposition," *IEEE Transactions on Geoscience and Remote Sensing*, vol. 57, no. 5, pp. 2583-2595, 2018.

[3] Q. Liu, C. Jiang, L. Jin, and S. Ouyang, "Detection of subsurface target based on FDA-MIMO radar," *International Journal of Antennas and Propagation*, vol. 2018, article no. 8629806, 2018

[4] R. Persico, G. Ludeno, F. Soldovieri, A. De Coster, and S. Lambot, "Improvement of ground penetrating radar (GPR) data interpretability by an enhanced inverse scattering strategy," *Surveys in Geophysics*, vol. 39, no. 6, pp. 1069-1079, 2018.

[5] F. Liu, C. Masouros, A. Li, T. Ratnarajah, and J. Zhou, "MIMO radar and cellular coexistence: a power-efficient approach enabled by interference exploitation," *IEEE Transactions on Signal Processing*, vol. 66, no. 14, pp. 3681-3695, 2018.
[6] F. Wen, D. Huang, K. Wang, and L. Zhang, "DOA estimation for monostatic MIMO radar using enhanced sparse Bayesian learning," *The Journal of Engineering*, vol. 2018, no. 5, pp. 268-273, 2018.
[7] Z. Cheng, B. Liao, Z. He, Y. Li, and J. Li, "Spectrally compatible waveform design for MIMO radar in the presence of multiple targets," *IEEE Transactions on Signal Processing*, vol. 66, no. 13, pp. 3543-3555, 2018.
[8] E. Tohidi, M. Coutino, S. P. Chepuri, H. Behroozi, M. M. Nayebi, and G. Leus, "Sparse antenna and pulse placement for colocated MIMO radar," *IEEE Transactions on Signal Processing*, vol. 67, no. 3, pp. 579-593, 2018.
[9] W. T. Lei and Y. J. Shi, "A windowed range migration imaging algorithm for ground penetrating radar applications," *Applied Mechanics and Materials*, vol. 477, pp. 1504-1508, 2014.
[10] H. Liu, Z. Long, B. Tian, F. Han, G. Fang, and Q. H. Liu, "Two-dimensional reverse-time migration applied to GPR with a 3-D-to-2-D data conversion," *IEEE Journal of Selected Topics in Applied Earth Observations and Remote Sensing*, vol. 10, no. 10, pp. 4313-4320, 2017.
[11] J. Yang, T. Jin, X. Huang, J. Thompson, and Z. Zhou, "Sparse MIMO array forward-looking GPR imaging based on compressed sensing in clutter environment," *IEEE Transactions on Geoscience and Remote Sensing*, vol. 52, no. 7, pp. 4480-4494, 2013.
[12] Z. Zeng, W. Li, J. Xi, L. Huangm, and Z. Wang, "Inverse direction imaging method of array type GPR based on DOA estimation," *Journal of Jilin University (Earth Science Edition)*, vol. 47, no. 4, pp. 1308-1318, 2017.

Qinghua Liu **https://orcid.org/0000-0002-1052-775X**

She received her B.Sc. degree in 1995 from Sichuan Normal University, M.Sc. degree in 2001 from Guilin University of Electronic Technology, and Ph.D. degree in 2014 from Xidian University. Now she is a professor in Guilin University of Electronic Technology. Her main research interest is radar signal processing.

Yuanxin He **https://orcid.org/0000-0003-2568-8772**

He received his B.Sc. degree in 2018 from Liren College of Yanshan University. Now he is studying for a master's degree at Guilin University of Electronic Technology. His main research interest is radar signal processing.

Chang Jiang **https://orcid.org/0000-0003-1405-7369**

He received his B.Sc. and M.Sc. degrees from Guilin University of Electronic Technology in 2016 and 2019, respectively. Now he is engaged in the research of signal processing and automatic driving at Guilin University of Electronic Technology.